A Survey of Quantitative Descriptors of Arterial Flows

Diego Gallo, Giuseppe Isu, Diana Massai, Francesco Pennella, Marco A. Deriu, Raffaele Ponzini, Cristina Bignardi, Alberto Audenino, Giovanna Rizzo and Umberto Morbiducci

Abstract Knowledge of blood flow mechanics is a critical issue (1) for an in depth understanding of the relationships between hemodynamic factors and arterial homeostasis and (2) for the identification of those flow features that lead to changes in the function and health of vessels. While from one side there is clear evidence that regions of disrupted flow are correlated to, e.g., the localization of atherosclerosis, the development of aneurysms and non-physiological transport of

D. Gallo (✉) · G. Isu · D. Massai · F. Pennella · M. A. Deriu · C. Bignardi · A. Audenino · U. Morbiducci
Department of Mechanics and Aerospace Engineering, Politecnico di Torino, 24 Corso Duca degli, Abruzzi 10129, Turin, Italy
e-mail: diego.gallo@polito.it

G. Isu
e-mail: giuseppe.isu@polito.it

D. Massai
e-mail: diana.massai@polito.it

F. Pennella
e-mail: francesco.pennella@polito.it

M. A. Deriu
e-mail: marco.deriu@polito.it

C. Bignardi
e-mail: cristina.bignardi@polito.it

A. Audenino
e-mail: alberto.audenino@polito.it

U. Morbiducci
e-mail: umberto.morbiducci@polito.it

R. Ponzini
HPC and Innovation Unit, CINECA, Via R. Sanzio, 4 20090, Milan, Segrate, Italy

G. Rizzo
IBFM, Research National Council, LITA Building—Via Fratelli Cervi, 93 20090, Milan, Segrate, Italy

R. Lima et al. (eds.), *Visualization and Simulation of Complex Flows in Biomedical Engineering*, Lecture Notes in Computational Vision and Biomechanics 12,
DOI: 10.1007/978-94-007-7769-9_1,

species, on the opposite cause-effect links still do not emerge clearly. To allow for a more effective and valuable understanding of blood flow structures and mechanisms in complex four-dimensional cardiovascular flows, in recent years a large number of hemodynamic parameters have surfaced in the literature, enabling the understanding of arterial hemodynamics and of the role of streaming blood in the development of pathological events. In this work, a survey of the currently adopted methods to characterize blood flow structures in arteries is presented and open questions (1) on their clinical utility and (2) on the inherent limitations in their in silico and in vivo application are discussed.

1 Introduction

The study of cardiovascular flows is of great interest because of the role of hemodynamics in cardiovascular diseases, the single largest cause of death worldwide and responsible for more than half of mortality in the developed countries. Several tools were developed for the interpretation and analysis of arterial hemodynamics. As a first approach, the study of arterial hemodynamics has relied in the past on simplification of the physics of the problem. For example, in 1775 Euler developed a series of equations which are nowadays widely adopted for the study of pressure wave propagation phenomena in the vascular tree (Euler 1775), or Poiseuille's Law has been used to model and represent blood flow motion (therefore ignoring pulsatility and simplifying the blood velocity profile shaped as parabolic). Another contribution was given by Womersley, whose description of pulsating flows allows to model and represent more complex flow patterns than the simple parabolic shape (Womersley 1955).

By late 1960s, Caro and others (1969) had shown that the localization of vascular diseases at arterial branches and bends could be explained by the presence of complex blood flow patterns at these sites. Subsequent studies have shown that the local flow behaviour of blood is implicated in the formation of atherosclerotic plaques and of phenomena such as thrombogenesis, atherogenesis, endothelial damage, intimal thickening and hyperplasia (Karino and Goldsmith 1985; Ku et al. 1985; Giddens et al. 1993; Moore et al. 1994). The unfavourable hemodynamic environment is often referred to with the vague expression "disturbed flow", that is usually used to imply mechanisms such as (1) the modulation of the friction forces at the vascular luminal surface (Sun et al. 2007) and the consequent effects on endothelial functions, and (2) the regulation/alterations in the mass transfer and in the residence time near the wall of atherogenic particles.

In this context, the importance of the knowledge of accurate local blood flow factors emerged, clearly requiring for methods with the capability of characterizing the blood flow dynamics to ease the clinical interpretation of the disturbed flow. Thus, the research on the role of the hemodynamics in vascular disease could take advantage of methods of data reduction that allow quantitative assessments

and comparisons. A variety of hemodynamic descriptors has been proposed over the years to (1) reduce the inherent complexity of the four-dimensional blood flow fields, (2) simplify the understanding of the flow dynamics, and (3) quantify hemodynamic disturbances as potential indicators of vascular wall dysfunction.

In the past, the majority of the studies on this subject focused primarily on wall shear stress (WSS, i.e., the force per unit area the flowing blood exerts on the endothelial cells lining the vessel lumen) as quantitative indicator of disturbed flow (Ku et al. 1985; Giddens et al. 1993). A large variety of parameters based on WSS has been proposed over the years and employed in a relevant number of studies. Only recently the interest in the role played by the bulk flow in the development of the arterial disease has grown. Thus, descriptors with the capability of quantifying phenomena depending on the complexity of the blood flow in the bulk are of great interest as they can offer insights, complement, integrate and extend the information given by the WSS-based descriptors.

Here we present a review of the currently adopted methods to characterize and classify blood flow structures in arteries. After a brief introduction about the importance of WSS and its role in vascular wall pathologies, established descriptors based on WSS, proposed over the years to quantify flow disturbances, are presented. Then, the role of bulk flow in arterial hemodynamics is discussed and different descriptors used to characterize bulk flow dynamics are introduced. Finally, examples of the applications of the reviewed descriptors are reported and the utility and perspective use of the introduced hemodynamic descriptors in the clinical practice are discussed.

2 On the Importance of Wall Shear Stress (WSS)

The fluid forces acting on the vessels' walls are thought to be capable of stimulating the endothelium to produce several cellular factors that can inhibit or promote inflammatory events (Yoshizumi et al. 2003). In vitro and in vivo studies on endothelial cells have shown contrasting effects between laminar shear flow with a definite direction (e.g., as seen in the straight part of the arterial tree) and the "disturbed" shear (e.g., as seen at arterial branch points and curved regions) in terms of their signal transduction, gene expression, structure, and functions (Chien 2007; Chiu and Chien 2011). Evidence from in vitro and in vivo studies suggests that both low WSS and highly oscillatory patterns of WSS cause intimal wall thickening (Caro et al. 1969; Friedman et al. 1981; Ku et al. 1985; Glagov et al. 1988; Moore et al. 1994; Pedersen et al. 1997; Malek et al. 1999), as seen at sites with such characteristics as curvatures, bifurcations, tortuosity and branching (in general where flow velocity and shear stress are reduced and flow departs from unidirectional patterns) (De Bakey et al. 1985). WSS can change the morphology and orientation of the endothelial cell layer: endothelial cells subjected to a laminar flow with high levels of WSS tend to elongate and align in the direction of flow, whereas in areas of low and oscillatory WSS, endothelial cells look more

polygonal without a clear orientation, with a lack of organization of the cytoskeleton and intercellular junctional proteins (Galbraith et al. 1998). In addition, it has been hypothesized that low WSS and the resultant stagnation of blood permit prolonged contact of the vessel wall with platelets, granulocytes, and metabolites that influence vascular homeostasis (Glagov et al. 1988; Shaaban and Duerinckx 2000). An overview of the current knowledge on vascular mechanobiology from a cellular to a tissue scale is reported by Chiu and Chien (2011). Indeed, the importance of shear stress oscillation at the wall for the physiology of the mechanosensitive endothelial cells has been pointed out by several authors, often providing indices to quantify these occurrences.

2.1 Metrics for Quantitative Hemodynamics: Hemodynamic Wall Descriptors

Various metrics have been proposed over the years to quantify WSS disturbances by using metrics originally focused on WSS magnitude. The hemodynamic wall parameters (HWPs) have then incorporated the information about spatial gradients of WSS and about the temporal variations of WSS time–varying profiles evaluating their harmonic content (Lee et al. 2009). Among the proposed HWPs, we report in the followings the most used ones.

1. Time Averaged Wall Shear Stress (TAWSS)

$$\mathrm{TAWSS} = \frac{1}{T}\int_0^T |\mathbf{WSS}| \cdot dt \tag{1}$$

where T is the time interval during which the values of the WSS vector are measured. Low TAWSS values (lower than 0.4 N/m^2) are known to stimulate a proatherogenic endothelial phenotype and are associated with intima/media complex thickening, whereas moderate (greater than 1.5 N/m^2) TAWSS values induce quiescence and an atheroprotective gene expression profile (Malek et al. 1999). Higher TAWSS values (greater than $10 \div 15$ N/m^2, relevant from $25 \div 45$ N/m^2) can lead to endothelial trauma and hemolysis (Kessler 2002).

2. Oscillatory Shear Index (OSI)

$$\mathrm{OSI} = 0.5\left[1 - \left(\frac{\left|\int_0^T \mathbf{WSS} \cdot dt\right|}{\int_0^T |\mathbf{WSS}| \cdot dt}\right)\right] \tag{2}$$

OSI is used to identify regions on the vessel wall subjected to highly oscillating WSS directions during the cardiac cycle. Low OSI values occur at sites where flow disruption is minimal, whereas high OSI values (with a maximum of 0.5) highlight sites where the instantaneous WSS deviates from the main flow direction in a large fraction of the cardiac cycle, inducing perturbed endothelial

alignment (He and Ku 1996). Although the OSI can identify regions of flow reversal, it is insensitive to shear magnitude. Sites where the TAWSS is low may be characterized by significant OSI but not necessarily, indeed low shear can result from flow expansion, which may follow from pulsatility, without any local flow reversal. Similarly, strongly oscillatory flows can exhibit the same OSI as very slow flows with the same waveform. As stated by Himburg et al. (2004), it seems unlikely that endothelial cells sense OSI per se. Several investigators, using histological data (Keynton et al. 2001; Goubergrits et al. 2002), demonstrated that only the presence of low and oscillating WSS favours the atherosclerotic plaque formation, while if TAWSS is next to the physiological range ($1 \div 2$ N/m^2), the intimal thickness is normal. These considerations suggest that OSI might better be employed in combination with other shear measures, rather than as a stand-alone index.

3. Relative Residence Time (RRT)

$$\mathrm{RRT} = \frac{1}{(1 - 2 \cdot \mathrm{OSI}) \cdot \mathrm{TAWSS}} = \frac{1}{\left| \int_0^T \mathbf{WSS} \cdot dt \right|} \tag{3}$$

RRT is inversely proportional to the magnitude of the time-averaged WSS vector (i.e., the term in the numerator of the OSI formula). Himburg et al. (2004) demonstrated that the residence time of particles near the wall is proportional to a combination of OSI and TAWSS. RRT is simply another type of time-averaged WSS, but inverted and with a more tangible connection to the biological mechanisms underlying atherosclerosis (Himburg et al. 2004). Indeed, Lee and colleagues (Lee et al. 2009) recommended RRT as a robust single metric of "low and oscillatory" shear.

4. WSS Spatial Gradient (WSSG)

$$\mathrm{WSSG} = \frac{1}{T} \int_0^T \sqrt{\left(\frac{\partial \mathbf{WSS}_p}{\partial p} \right)^2 + \left(\frac{\partial \mathbf{WSS}_n}{\partial n} \right)^2} \cdot dt \tag{4}$$

where p and n are the directions respectively parallel and normal to the direction of the time-averaged WSS vector. Thus, WSSG is calculated starting from the WSS gradient tensor components. Proposed by De Paola et al. (1992), the WSSG may be considered a marker of endothelial cell tension. Large sustained WSS gradients produce endothelium dysfunction due to the aggravating effects of spatially changing hemodynamic forces.

5. WSS Angle Gradient (WSSAG)

$$\mathrm{WSSAG} = \frac{1}{T} \frac{D}{\pi} \int_0^T |\nabla \Phi_n| \cdot dt \tag{5}$$

where D is the vessel diameter, and Φ_n is the scalar field of WSS angle deviations:

$$\Phi_n = \arccos\left(\frac{\mathbf{WSS}_i \cdot \mathbf{WSS}_j}{|\mathbf{WSS}_i|\,|\mathbf{WSS}_j|}\right) \tag{6}$$

where $\mathbf{WSS}_i$ is the WSS vector at the location of interest and subscript j is an index for the surrounding stress vectors. Longest and Kleinstreuer (2000) proposed the WSSAG to highlight regions exposed to large spatial variations in the mean WSS direction, irrespective of magnitude. Areas with high WSSG are thought to be related to intimal hyperplasia (Bunchanan and Kleinstreuer 1998): significant and sustained WSSAG values tend to handicap the endothelial cell response initiating the process of atherosclerosis.

6. Dominant Harmonic (DH)

$$\mathrm{DH} = \max\left(F_{|\mathrm{WSS}|}\left(n\frac{2\pi}{T}\right)\right), n \in \mathbf{N}^+ \tag{7}$$

where $F_{|\mathbf{WSS}|}$ is the Fourier-transform of the time-varying waveform of the WSS magnitude and n is a positive integer. The DH is thus obtained through the Fourier decomposition of the WSS magnitude profiles along the cardiac cycle and it is defined as the harmonic with the highest amplitude. Himburg and Friedman (2006), proposing this descriptor, suggested that the frequency spectrum of WSS time-varying profiles could play a role in the atherosclerotic lesion development.

7. Harmonic Index (HI)

$$\mathrm{HI} = \frac{\sum_{n=1}^{\infty} F_{|\mathbf{WSS}|}\left(n\frac{2\pi}{T}\right)}{\sum_{n=0}^{\infty} F_{|\mathbf{WSS}|}\left(n\frac{2\pi}{T}\right)}, n \in \mathbf{N}^+ \tag{8}$$

The descriptor HI, whose value ranges from zero to one, was proposed by Gelfand et al. (2006) as a measure of the relative contribution to the harmonic amplitude spectrum of non-stationary intensity to the overall signal intensity. In this way, it is possible to evaluate the relative contribution of the pulsatile component of the WSS magnitude.

For practical purposes, many of the proposed HWPs provide essentially the same information and therefore can be considered redundant. Lee et al. (2009), adopting a computational dataset made of 50 carotid bifurcation models, tested for correlations among a large variety of HWPs. Their comprehensive evaluation demonstrated that RRT can be used as single marker of low and oscillatory shear, and issues are questioned about the harmonic-based HWPs, related to their definition in the presence of strongly non-axial flows (Lee et al. 2009). Thus, we here iterate their recommendation to adopt RRT to localize areas of disturbed shear on the vessel wall.

3 On the Importance of Bulk Flow

Most mechanisms promoting degenerative phenomena and pathologies affecting vascular districts deal with three- and four-dimensional phenomena. In addition, the bulk flow plays a key role in determining WSS patterns. Notwithstanding, the focus of the most part of the studies in the literature is almost exclusively on WSS-based metrics as quantitative indicators of disturbed flow. In the past, the potential role of bulk flow in the development of arterial disease was scarcely investigated. This is partially due to the scarcity of robust quantitative descriptors of bulk flow with the ability of operating a reduction of the inherent complexity associated to four-dimensional flow fields in realistic geometries.

Recently, several studies both in silico and in vitro (Stonebridge et al. 1996; Grigioni et al. 2005; Morbiducci et al. 2007a, b; Fan et al. 2008; Chen et al. 2009; Liu et al. 2009; Zheng et al. 2009; Zhan et al. 2010) have renewed with quantitative results the presumption that arterial bulk flow could elicit the fluid-wall interaction processes leading to the onset of vessel wall pathologies (Ku and Giddens 1983; Caro et al. 1996; Stonebridge et al. 1996; Malek et al. 1999; Grigioni et al. 2005; Augst et al. 2007; Morbiducci et al. 2007a, b; Caro et al. 2009). These studies, in light of the observation that unfavourable effects like alterations in mass transfer and particle residence times are strictly related to bulk flow effects, especially when blood flow is complex, suggest that WSS-based analysis should be complemented by a quantitative description of the bulk flow and that such a description represents a potential source of information.

In order to investigate the relationships between particular blood flow patterns and physiopathological events, helicity has recently gained recognition as able to describe the arrangement of blood streams in complex patterns (Morbiducci et al. 2007b). The use of helicity to analyse bulk flow features has been applied by several groups to different cardiovascular districts (see for example Morbiducci et al. 2007b; Fan et al. 2008; Chen et al. 2009; Liu et al. 2009; Morbiducci et al. 2009a, 2010, 2011; Liu et al. 2010, 2011; Zhan et al. 2010; Lorenz et al. 2012). Helicity is a measure of the alignment of the velocity and the vorticity vectors (Moffatt 1969) and it represents the potential for helical flow, i.e., flow with a corkscrew-like pattern, to evolve. Helical flow is the product of the composition of translational and rotational motion and its role in vascular hemodynamics has long been debated.

In the past, it was postulated that helical flow has a relevant importance in the physiology of the vessel, preventing stagnation zones and flow separation at the arterial walls. In the 1990s, researchers put forward hypotheses on the theoretical advantages derived from helical blood flow (Stonebridge et al. 1996). Frazin et al. (1990) put forward the idea of a relationship between the shear forces caused by rotational flow and both the deposition of atherosclerotic plaque and the direction and extent of aortic dissection. In the aortic arch, Kilner et al. (1993) suggested that the stability induced by helical flow in the upper aortic arch spares this region from the tendency for plaques to form, whereas more unstable flow patterns

predispose to atherosclerosis; Bogren and Buonocore (1999) observed the presence of helical flow regardless the age of the volunteers. Houston and colleagues (Houston et al. 2003) found that carotid atheromatous disease is associated with a reduction in the prevalence of a systolic helical flow pattern in the aortic arch. Helical flow may also account for a significant amount of normal organ perfusion (Frazin et al. 1996) from branch vessels due to the centripetal spin (i.e., imparted tangential velocities) induced in blood. Moreover, an absence of aortic helical flow might be a predictor of renal impairment deterioration in patients with renal artery stenosis (Houston et al. 2004). In 2007, Morbiducci and colleagues (Morbiducci et al. 2007b), investigating the existence of a relationship between helical flow structures and vascular wall indexes of atherogenesis in aortocoronary bypass models, found that an arrangement of the flow field in helical patterns may elicit a damping in shear stress effects on the vessel wall. Chen and colleagues (Chen et al. 2009) found that intentional induction of helical flow in an endovascular stent reduced the size of the disturbed flow zones, enhanced the average wall shear stress, and lowered wall shear stress oscillations, which are adverse factors involved in the development of arterial restenosis after stent deployment; the same group (Liu et al. 2010) observed that the helical flow in the aorta may have great influence on the distribution of the luminal surface concentration of low density lipoproteins and, as a consequence, on the spatial distribution of atheromatous plaques. Very recently, Gallo and colleagues demonstrated that a high amount of helical flow suppresses the disturbed shear at the normal carotid bifurcation, but this beneficial effect is moderated when one direction of rotation is predominant in the flow field (Gallo et al. 2012a).

From a phenomenological viewpoint, an arrangement of the bulk flow in complex helical patterns might play a significant role in the tuning of the cells mechano-transduction pathways. It is likely that for highly helical flows, the conservation laws within the Navier–Stokes equation inhibit the transfer of helicity down the length scales, and thus the process through which energy is transferred (Ditlevsen and Giuliani 2000). As a result of this inhibition, helical energy may affect the focal contact between endothelial cell and the monocyte within the flow, i.e., helical structures could elicit the convective dispersion of monocytes within the vessel at all scales, due to the complex three-dimensional flow pattern. Furthermore, the stability induced by helical flow and the decrease in laterally directed forces may reduce turbulence in the tapering branching arterial tree and at stenoses (Caro et al. 2002). Several authors emphasize the existence of a relationship between helical flow patterns and transport phenomena affecting blood–vessel wall interaction (Pritchard et al. 1995); Hsiai et al. 2003; Morbiducci et al. 2007b; Zhan et al. 2010). These processes are fundamental to the initiation of inflammatory responses, due to alterations in the residence time of atherogenic particles (Caro et al. 1971; Friedman et al. 1987). Moreover, bulk flow structures are primarily responsible for mass transfer (Caro et al. 1969; Ma et al. 1997), in particular for those species within blood that take advantage of mixing induced by convection. For example, several studies identify the oxygen flux to the arterial wall to be another factor involved in the localization of atherogenesis (Santilli

et al. 1995; Sluimer et al. 2008), while recent studies has provided evidence for the existence of a relationship between shear-induced activation of platelets (Kroll et al. 1996) and metrics that give measures for the alignment of the local velocity and vorticity vectors (Morbiducci et al. 2009b; Massai et al. 2012).

According to these observations, it is clear that helical flow represents a natural feature of arterial hemodynamics and that a thorough understanding of the generation and disappearance of helical structures in the streaming blood is of great interest. In particular, helical flow could be used as a fluid dynamic signature for the identification of sites prone to fibrointimal thickening and atherosclerotic plaque formation (Gallo et al. 2012a).

3.1 Metrics for Quantitative Hemodynamics: Hemodynamic Bulk Flow Descriptors

Helicity can provide a better understanding of the role of pitches and torsions in the development of complex flow fields, describing and revealing the global organization of the flow.

By definition, the helicity *H(t)* of a fluid flow confined to a domain ***D*** of three-dimensional Euclidean space $\mathbf{R}^3$ is the integrated internal product of the local velocity vector and the local vorticity vector, and, being related to the magnitude of the nonlinear term in the Navier–Stokes equation (and geometrically characterizing the knottedness of vortex lines), it has a great influence on the evolution and stability of both turbulent and laminar flows (Moffatt and Tsinober 1992).

$$H(\mathbf{x},t) = \int_{\boldsymbol{D}} \mathbf{v}(\mathbf{x},t)\cdot\omega(\mathbf{x},t)dV = \int_{\boldsymbol{D}} H_k(\mathbf{x},t)dV \tag{9}$$

where $\mathbf{v}(\mathbf{x},t)$ and $\boldsymbol{\omega}(\mathbf{x},t)$ are the velocity and the vorticity vector, respectively, and their internal product H_k is the helicity density.

A useful indicator of how velocity field is oriented with respect to the vorticity field is given by the local value of the cosine of the angle between the velocity and vorticity vectors, obtained through the normalization of the helicity density H_k. In the past, the quantity Localized Normalized Helicity (LNH) has been proposed (Shtilman et al. 1985), defined as:

$$\mathrm{LNH}(\mathbf{x};t) = \frac{\mathbf{v}(\mathbf{x};t)\cdot\omega(\mathbf{x};t)}{|\mathbf{v}(\mathbf{x};t)||\omega(\mathbf{x};t)|} = \cos\varphi(\mathbf{x};t) \qquad -1 \le LNH \le 1 \tag{10}$$

where $\mathbf{v}$ is the velocity vector, ω the vorticity vector, $\mathbf{x}$ is the position and t the time instant. The non-dimensional quantity LNH is the local value of the cosine of the angle $\varphi(\mathbf{x};t)$, between the velocity and vorticity vectors: the absolute value of LNH can range between one, when the flow is purely helical, and zero, in general,

in presence of reflectional symmetry in the flow. Moreover, the sign of LNH is a useful indicator of the direction of rotation. Hence, LNH is a useful descriptor of changes in the direction of the rotation of flow into vessels during the cardiac cycle, because a local right/left-handed rotation can be identified by a change in sign of the local value of LNH.

The definition of the bulk flow quantities introduced in this section can be considered both as Eulerian or Lagrangian specifications of flow. In fact, a picture of the spatial distribution of them is known at each instant of time (i.e., they are function of position and time). On the other hand, they can be used to describe the dynamical path history of a fluid element, identified by its position at some initial time.

3.1.1 Eulerian Approach

Current in vivo (e.g., phase-contrast magnetic resonance imaging, PC MRI), in vitro (e.g., particle image velocimetry), and computational methods used for quantifying blood flow produce as output Eulerian velocity data, typically. The velocity field itself has limited clinical relevance, typically the interest relies in the transport of the fluid or in the forces produced by the fluid motion. The quantities defined in Eqs. 9 and 10 can be calculated in an Eulerian field, starting from the velocity field.

It is possible to define helicity bulk flow descriptors according to a Eulerian approach. Basic characteristics of helical structures, like their intensity, the balance between counter-rotating structures, and their size can be evaluated by using the following descriptors:

$$h_1 = \frac{1}{TV} \int_T \int_V H_k \, dV dt \tag{11a}$$

$$h_2 = \frac{1}{TV} \int_T \int_V |H_k| \, dV dt \tag{11b}$$

$$h_3 = \frac{h_1}{h_2} \tag{11c}$$

$$h_4 = |h_3| = \frac{|h_1|}{h_2} \tag{11d}$$

$$h_5 = \frac{\max(V_+, V_-)}{\min(V_+, V_-)} = \frac{V_d}{V_m} \tag{11e}$$

$$h_6 = \frac{\frac{1}{V_d}\int_T \int_{V_d} H_k \, dV\, dt}{\frac{1}{V_m}\int_T \int_{V_m} H_k \, dV\, dt} \tag{11f}$$

where V is the volume of fluid, V_+ (V_-) is the total volume of the helical structures rotating in the direction identified by the positive (negative) sign. The volumes V_+ and V_- identify the volume occupied by the dominant direction of rotation V_d and the volume occupied by the minor direction of rotation V_m. The descriptor h_1 is the time-averaged value of the helicity, normalized with respect to the volume of integration. By definition, h_1 equals 0 in the presence of reflectional symmetry in the fluid domain, for instance if the flow arrangement in the domain consists in symmetric counter-rotating helical structures, while when it has signed values, its sign indicates the predominant direction of rotation. The helicity intensity, given by the integration of the absolute value of H_k, defines descriptor h_2 and it is an indicator of the total amount of helical flow in the fluid domain, irrespective of direction. Descriptor h_3 is a non-dimensional quantity ranging between -1 and 1: its value equals -1 when only left-handed helical structures are present in the domain, it equals +1 when only right-handed structures are present and it equals 0 in case of reflectional symmetry. The focus on the balance between counter-rotating structures, neglecting what is the major direction of rotation, is given by descriptor h_4, defined as the absolute value of h_3 and thus ranging between 0 and +1. The descriptor h_5 is the ratio between the volumes of the helical structures in the dominant direction of rotation V_d and the minor direction of rotation V_m. The ratio of the helicity intensities in volumes V_d and V_m is given by descriptor h_6.

This approach has been adopted in a very recent study (Gallo et al. 2012a, b). Adopting a computational dataset composed of 50 normal carotid bifurcations, they calculated the six descriptors h_i and explored the relationship between the helicity-based Eulerian descriptors and the overall burden of abnormal WSS. The regression analysis underlined the importance of two descriptors (h_2 and h_4) quantifying the total helicity intensity in the domain and the ratio between the helicity intensity of the counter-rotating helical structures. Thus, a high amount of helicity in the carotid bifurcation flow field is instrumental in suppressing flow disturbances. However this protective effect can be moderated when one direction of rotation is dominant in the flow field. Hence, the onset of helical flow into the carotid bifurcation could avoid atheroprone hemodynamics, contributing to limit flow separation leading to low and oscillatory shear (Gallo et al. 2012a).

The advantages of a Eulerian specifications of those bulk flow quantities reside mainly in the attractiveness of this approach for clinicians, due to its immediateness. Eulerian quantities in fact have a simpler definition, allows real-time analysis and can give a picture of the entire flow field. Although is often reasonable to infer the bulk fluid motion from inspection of the velocity data, a quantification of the flow structures in unsteady flows (i.e., when the time history of the velocity field has to be taken into account also) could be difficult and could result in misinterpretations.

3.1.2 Lagrangian Approach

Hemodynamic quantities such as residence times of individual fluid particles, particle deposition, and particle shear exposure can be evaluated according to Lagrangian specifications because they rely on knowledge of the dynamical path history of a fluid element, and the Lagrangian characterization identifies the element by its position at some initial time. They hence differ from other hemodynamic quantities such as WSS, which can be addressed using Eulerian specifications because a picture of the spatial distribution of these quantities is known at each instant of time (i.e., they are functions of position and time).

Since the very first eminent studies, in order to extract Lagrangian hemodynamic information, a one-way coupled Eulerian/Lagrangian method was proposed, in which the effect of a particle's motion on the surrounding flow field is neglected (Ehrlich and Friedman 1977; Perktold and Resch 1990): in this way the Lagrangian approach simply reduced to computing the particle trajectories from the pre-computed Eulerian flow field.

In principle, to model blood flow in large arteries, particle-seeding scheme reflecting the physiological distribution of blood corpuscles should be used. However, the concentration of particles required to model the physiological situation would present extreme computational demands: the concentrations make the computational cost of the particle motion modelling unfeasible (Tambasco and Steinman 2001, 2002). Hence, these limitations force to employ alternative approaches for the computation of meaningful path-dependent hemodynamic quantities for arterial models of blood flow. Among them, the most cost-effective seems to be the statistical approach, consisting of extracting the relevant quantities from ensemble averages over a sufficient set of particles.

In general, Lagrangian derived parameters can be used in the study in a wide range of arterial models of quantities of interest such as particle deposition, particle stress history (e.g., to investigate blood trauma) and, very recently, the level of pitch and torsion in the flow development, obtained through helicity (Hyun et al. 2000, 2001; Kleinstreuer et al. 2001, Tambasco and Steinman 2001, 2002; Hyun et al. 2004; Grigioni et al. 2005; Morbiducci et al. 2007a, b).

Recently a four-dimensional descriptor, the Helical Flow Index (HFI), has been introduced in order to get a "measure" of the helical structure in the blood flow. Originally developed and applied to computational models (Grigioni et al. 2005, Morbiducci et al. 2007a, b), and very recently tested in vivo on 4D PC-MRI measurements in the human aorta (Morbiducci et al. 2009a, 2011), the HFI represents the content of helical motion by clustering the information according to a Lagrangian analysis of the flow. Previous studies demonstratedthat HFI is an effective synthetic flow descriptor of complex, fully four-dimensional flow fields (Morbiducci et al. 2007a, b, 2011).

Technically, the HFI is defined using the LNH as basic quantity. Considering the trajectory described by the generic particle k moving in a vessel, its dynamics can be characterized by means of the quantity:

$$hfi_k = \frac{1}{(t_k^{end} - t_k^{start})} \int_{t_k^{start}}^{t_k^{end}} |\mathrm{LNH}_k(\varsigma)| \mathrm{d}\varsigma \tag{12}$$

Equation 12 is the integral sum, in time, of the LNH values experienced by the *k-th* particle moving during the time interval $\left(t_k^{end} - t_k^{start}\right)$.

Over the N_p ($k = 1,\ldots, N_p$) particles moving in the fluid domain, the HFI can be calculated as:

$$\mathrm{HFI} = \frac{1}{N_p} \sum_{k=1}^{N_p} hfi_k \qquad 0 \leq \mathrm{HFI} \leq 1 \tag{13}$$

The previous hemodynamic quantities (Eqs. 12, 13) are considered Lagrangian specifications of flow since they depend on knowledge of the dynamical path history of a piece of fluid element.

The Lagrangian approach, that allows to extract path dependent quantities tracking the fluid particle, in conjunction with visualization techniques, is particularly useful for characterizing unsteady flow patterns, and for highlighting important hemodynamic features. Particle traces offer three-dimensional visualization of flow patterns which have proven to be useful tools to interrogate complex flow fields in vessels and in general to reveal global organization of the flow (Steinman 2000; Morbiducci et al. 2007a, b; 2009a, b), making easier to detect by visual inspection the relevant flow features and to understand the true fluid motion. The definition of path dependent quantities allows the investigation of dynamical path histories and could offer a practical way to divide the particles into groups regardless of position (e.g., using threshold for visualization). On the other hand, the main disadvantages of a Lagrangian approach are a high computational cost, the convectiveness of the particles, resulting in a poor control over the zone of investigation that is determined by the particle motion and accumulation. Furthermore, the influence of particle distributions and of particle seeding schemes on quantities of interest is poorly investigated. Finally, adopting a Lagrangian approach it is difficult to get a complete picture of the flow at specific time instants.

Alternatively to fluid motion tracking by computing particle trajectories through velocity data integration, it is worth mentioning the recently proposed use of the finite-time Lyapunov exponent (FTLE) to characterize flow kinematics of unsteady flows. The FTLE measures the maximum linearized growth rate of the distance between initially adjacent fluid particles, tracked over a finite time interval (Haller 2001), and its calculation yields a scalar field derived from fluid trajectories. Ridges of local maxima in the FTLE fields are able to reveal flow features, identifying Lagrangian coherent structures (Shadden et al. 2005; Shadden and Taylor 2008). For example, Shadden and Taylor (2008) and Vetel et al. (2009) adopted this approach to visualize helical structures, vortex boundaries, flow recirculation and flow separation regions in the human carotid artery.

4 Hemodynamic Descriptors: Examples of in silico and in vivo Applications, Their Significance and Limitations

Nowadays, the coupling of medical imaging and computational fluid dynamics (CFD) is used to obtain a realistic detailed description of the local hemodynamics. This kind of image-based analysis is applied to study vascular districts with marked predilection to vascular pathologies (Taylor and Steinman 2010), like the carotid artery and the thoracic aorta. In the followings, we report two example of image-based in silico and in vivo calculation of the introduced hemodynamic descriptors.

As a first example, we adopted the anatomically realistic computational model of a human carotid artery developed by Morbiducci and colleagues (Morbiducci et al. 2010). Exhaustive details about the geometry reconstruction, the computational setup and the CFD simulations can be found in (Morbiducci et al. 2010).

In Fig. 1 we show different ways of visualizing the flow patterns within the vessel. All the panels are representations of the same data, but the information conveyed is different. From the observation of Fig. 1, it can be noticed that OSI (panel A), TAWSS (panel B) and RRT (panel C) capture flow disturbances at the same sites of the bifurcation, highlighting the bifurcation bulb site as the surface area exposed to a higher risk. Helicity in the bulk flow can be visualized with a Eulerian static depiction (Fig. 1, panel D) or a Lagrangian dynamic depiction (Fig. 1, panel E). The Eulerian representation of LNH isosurfaces (Fig. 1, panel D) is representative of the flow arrangement within the volume of the bifurcation, going into detail about the formation of helical blood structures: counter-rotating coherent helical structures arise at the base of the daughter vessels in correspondence of the bulb. The particle traces, coloured by means of instantaneous value of LNH, highlight the onset of a recirculation region and a flow separation region in correspondence of the bifurcation bulb, qualitatively in accordance with the localization given by the HWPs (Fig. 1, panel E).

A second example regards the evaluation of the HWPs in a CFD model of thoracic aorta. Details are given in Gallo et al. (2012b) and Morbiducci et al. (2013). TAWSS, OSI, and RRT distributions mainly capture flow disturbances at the same sites, even though differences are present. In detail, they identify, as regions of disturbed shear, areas on the curvature of the arch and focal regions in the distal descending aorta (Fig. 2).

In the same subject, an in vivo evaluation of HFI was performed (Morbiducci et al. 2009a, 2011). The particle traces in Fig. 3 show that the flow arrangement is strongly characterized by the onset of coherent helical structures. Two large counter-rotating helical structures arise in the proximal region of the outer wall and develop towards the inner wall of the arch (Fig. 3).

This simple example demonstrates that it is possible to quantify arterial bulk flow features in vivo with techniques that are mature for the application in the clinical practice. This opens an intriguing scenario. In order to perform large scale

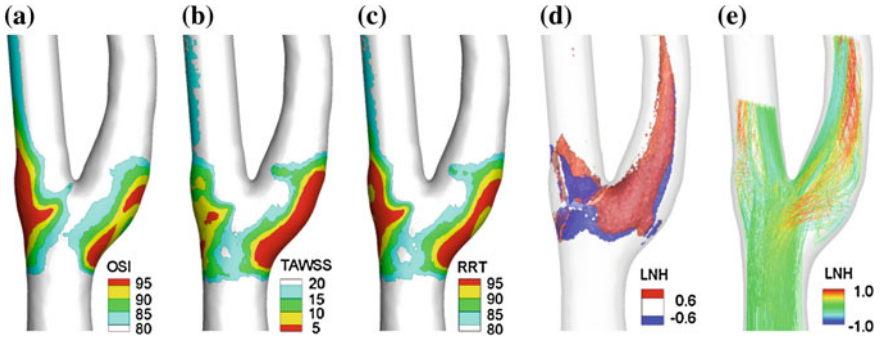

Fig. 1 Synoptic representation of the presented approaches. *Panel* **a**, **b** and **C** depict OSI, TAWSS and RRT distributions, respectively. *Colour-code* indicates areas exposed to OSI and RRT values above the 80th, 85th, 90th and 95th percentile values over the bifurcation surface area (*panel* **a** and **c**), and areas exposed to TAWSS values above the 5th, 10th, 15th and 20th percentile values (*panel* **b**). *Panel* **d** shows a Eulerian representation of bulk flow helicity using LNH iso-surfaces at the beginning of the cardiac cycle. *Panel* **e** displays a Lagrangian representation of helicity: particles injected at the beginning of the systole are tracked during the entire cardiac cycle. Each particle trace is colour-coded with respect to LNH values

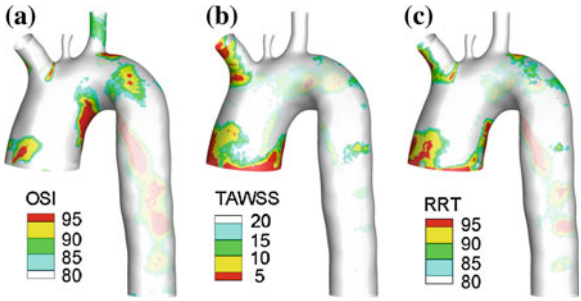

Fig. 2 *Panel* **a**, **b** and **c** depict OSI, TAWSS and RRT distributions, respectively. *Colour-code* indicates areas exposed to OSI and RRT values above the 80th, 85th, 90th and 95th percentile values over the bifurcation surface area (*panel* **a** and **c**), and areas exposed to TAWSS values above the 5th, 10th, 15th and 20th percentile values (*panel* **b**)

studies of hemodynamic risk in vessel wall pathologies, the ideal descriptors should be easily measurable in vivo. The use of routinely-acquired clinical data from which it is possible to infer the amount of disturbed flow would allow to investigate the hemodynamic risk of vessel pathologies in large-scale studies and in the clinical practice. Although great advances have been made in the area of image-based CFD, such models are still cumbersome, time-consuming to construct and use, and affected by a certain number of assumptions.

In vivo WSS estimate has been recently proposed, mainly by four-dimensional phase contrast MRI (4D PC MRI), through which it is possible to directly acquire 3D and three-directional data on blood flow over time. However, several

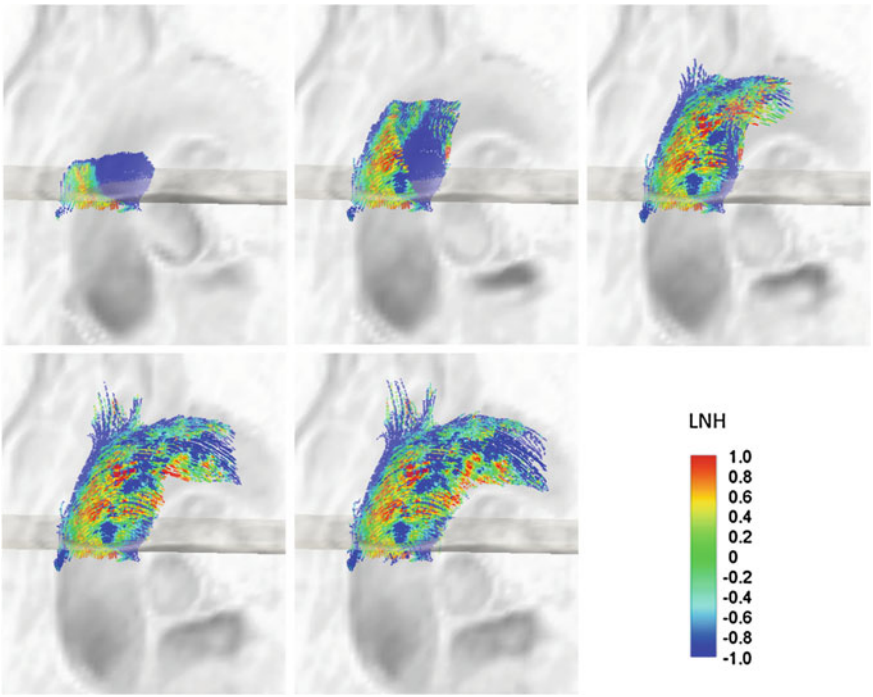

Fig. 3 Evolution of particle sets emitted during the flow deceleration phase in the thoracic aorta. *Color-coding* of the particle traces was used to display the instantaneous LNH value. The evolution is pictured at time intervals of 0.152 s

limitations affect the accuracy of the results. Since WSS depends on the spatial velocity gradient at the vessel wall, it can be calculated from the MRI-measured velocity fields, but limited spatial and temporal resolution, limited signal-to-noise ratio, the difficulty of accurately segmenting the moving vessel lumens, partial volume effects, and numerical derivation of the velocity field are likely to introduce inaccuracies in the estimations of WSS.

To evaluate in vivo WSS, the main image parameters (in-plane pixel size, slice thickness, number of time frames per cardiac cycle) must be selected according to conflicting constraints. On one hand, they must be able to capture the flow features within the vascular site of interest. On the other hand, the technological limitations of MRI scanners bind the achievable image resolution in clinical practice, where a trade-off policy is pursued by minimizing the overall costs and scanning time to ensure the minimal requirements for diagnostic purposes. These clashing constraints become critical when the advanced processing of in vivo blood flow datasets required to evaluate WSS is attempted. In fact, the application of numeric algorithms including, for example, data interpolation, requires not only low noisy data, but also spatial and temporal sampling rates sufficient to avoid the introduction of a consistent source of numerical errors. In general, the definition of the

optimal in vivo data sampling rate is challenging, since it depends on the complexity of the sampled field and on the 'regularity' of the data, which is not well defined a priori. At the moment, the environments traditionally used for validating protocols, such as in vitro or theoretical models, do not give definitive solutions to the problem, due to inherent limitations. In vitro validation is limited by costs, time consumption, proper experimental setup to be built, intrinsic source of noise and/or artefacts such as eddy currents, concomitant gradients, displacement, misregistration, partial volume effects, intra-voxel phase dispersion and aliasing. As for theoretical models, they remain extremely simplistic descriptors of cardiovascular flows.

Frydrychowicz et al. (2011) in their excellent review underlined that WSS estimates from 4D PC MRI measurements are restricted by a spatial resolution between 1.4 and 2.4 mm that produces a WSS underestimation of one order of magnitude when compared to CFD WSS maps (Frydrychowicz et al. 2011). Boussel et al. (2009) stated that "Although 4D MRI can provide a rough estimate of WSS, it is not currently capable of providing accurate absolute measurements", and Markl et al. (2010) affirmed that the current spatiotemporal resolution of flow-sensitive 4D MRI can considerably underestimate the true WSS magnitude, thus limiting the accuracy of wall parameter calculations.

The main problems arising from WSS in vivo calculations are the followings:

- MR measurements show poor sensitivity to low values of velocities. The sensitivity is governed by the setting chosen for the velocity encoding level (VENC). It is usual for the VENC to be set sufficiently high to avoid aliasing in regions with the highest velocity; but in this way the velocity to noise ratio is compromised in regions of slow flow, generally located at the boundary of the lumen. Zhao et al. (2002) showed that MR measurements in a carotid bifurcation phantom produced spurious velocity vectors in the near-wall region. Given the fact that WSS is a function of near wall velocity gradients, they concluded that WSS evaluated directly from the MR data might not be reliable at certain locations. These limitations are only partially overcome by the recent diffusion of systems with multiple VENCs. Another problem is signal loss due to intra-voxel dephasing in regions of complex flow (Papathanasopoulou et al. 2003). Unfortunately, these are precisely the regions of most interest.
- In addition to sources of errors in velocity measurement, the relatively low spatial and temporal resolution of MRI results in an averaging of the measured velocities which strongly impacts the calculated values of the velocity gradients. The effects of spatial averaging resulting from limited spatial resolution are particularly evident in regions with a broad distribution of velocities within a single voxel, such as at the edge of vessels. Temporal resolution is also an important factor. Indeed, current implementations of 4D MRI have relatively low temporal resolution. Temporal averaging consists in velocity averaging through time, reducing the ability of MRI to estimate transient events, and in a substantial smoothing of the shear values particularly when these values are high, i.e., in regions of rapid spatial change in velocity. To overcome resolution

limitations, a longer time scan would permit an improvement of the resolution but it also increases the likelihood of patient motion, which can substantially degrade the measurements. Imaging at high field strengths would provide increased signal-to-noise ratio which could be used either to reduce imaging time by the use of higher acceleration factors, or to improve resolution, although errors in velocity measurements that result from scanner imperfections at higher field strengths are not yet well characterized.

- WSS calculation relies on lumen edge definition on the magnitude image of the PC MRI which is often difficult to delineate. The precise identification of the blood vessel wall boundary within the image pixel is difficult due to limited resolution, and because that pixel may be partially covered with moving blood and partially covered by the stationary vessel wall (Shaaban and Duerinckx 2000). Inadequate spatial resolution leads to partial volume effects at the vessel walls and a limited number of velocity data points from which to estimate the wall position. This results in errors in wall position and in local surface orientation, degrading the WSS calculation. This is exacerbated when noise is included from surrounding structures which is particularly pronounced if that structure has little or no magnetization (e.g., air). Morbiducci et al. (2012) observed, using a synthetic PC MRI dataset, that image processing steps involving spatial and temporal interpolation of local velocity values to reconstruct the vessel wall could lead to unreliable direct estimation of WSS from PC MRI in vivo data. Fatemi and Rittgers (1994) compared polynomial curve fitting from first through eighth order, and found that while lower-order polynomials fail to capture important velocity profile information, higher-order approximations result in unpredictable results due to oscillations of the fitting functions. Moreover, WSS calculation requires a selection of velocity vectors close to the wall, and it is important to use a reasonable estimate of that distance as it can affect the results. Results from Long et al. (2004) indicate that shear rate determined at 250–300 μm from the wall will underestimate WSS by about 10 %.

Hence, direct accurate estimation of WSS from MR measured velocities is not a viable option for in vivo applications just yet. A number of issues need to be resolved. Developments in hardware are expected to reduce, though not entirely eliminate, these effects but WSS in vivo estimation remains a significant technical challenge.

As described previously, in recent years the computation of bulk flow quantities has emerged as a possible strategy to describe the temporal and spatial complexity of arterial blood flow and complement WSS-based atherogenic hemodynamic classification (Morbiducci et al. 2010). Morbiducci et al. (2012) have demonstrated using a synthetic PC MRI dataset the reliability of measured bulk flow hemodynamics at spatial and temporal resolutions that can be adopted in the clinical practice. They also showed that the higher reliability of bulk flow quantities with respect to WSS-based descriptors could make the calculation of 4D bulk flow

descriptors an outcome which is less sensitive to the image resolution and might be more suitable for in vivo application (Morbiducci et al. 2012).

Very recently, several authors successfully quantified helicity-derived quantities in vivo from time resolved phase-contrast measurements. Morbiducci and colleagues (Morbiducci et al. 2009a, 2011) quantified helical flow in vivo in the human thoracic aorta according to a Lagrangian approach: particle traces were calculated from velocity data and characterized calculating the LNH. Harloff et al. (2009) visualized and quantified helical flow from MRI measurements in carotid artery, even though helical flow was categorized only based on the direction of rotation (qualitative analysis). Lorenz et al. (2012) quantified in vivo the temporal average of the normalized mean helicity on cross-sections in thoracic aorta, by using helicity density and applying schemes previously tested in silico (Grigioni et al. 2005).

5 Conclusions and Future Directions

The purpose of this chapter was to give an overview on the existing methods for quantifying disturbed flow in arterial hemodynamics. Rather than providing a comprehensive list of all the available approaches, we tried to organize this wide matter in lights of the recent developments and the perspective use of these quantities. Our aim was to provide the reader with the means for choosing the best descriptor for the specific problem at hand. An important issue to be explored in the future is the incorporation of hemodynamic descriptors (i.e., based on fluid dynamics information) in appropriate measures of performance for surgical interventions, device optimization, follow-up studies on subjects undergoing surgical procedures (Marsden et al. 2008).

References

Augst AD, Ariff B, Thom SA, Xu XY, Hughes AD (2007) Analysis of complex flow and the relationship between blood pressure, wall shear stress, and intima-media thickness in the human carotid artery. Am J Physiol Heart Circ Physiol 293:H1031–H1037

Bogren HG, Buonocore MH (1999) 4D magnetic resonance velocity mapping of blood flow patterns in the aorta in young vs. elderly normal subjects. J Magn Reson Imaging 10:861–869

Boussel L, Rayz V, Acevedo-Bolton G, Lawton MT, Higashida R, Smith WS, Young WL, Saloner D (2009) Phase-contrast magnetic resonance imaging measurements in intracranial aneurysms in vivo of flow patterns, velocity fields, and wall shear stress: comparison with computational fluid dynamics. Magn Reson Med 61(2):409–417

Buchanan JR , Kleinstreuer C (1998) Simulation of particle-hemodynamics in a partially occluded artery segment with implications to the initiation of microemboli and secondary stenoses. J Biomech Eng 120(4):446–454

Caro CG, Fitz GJ, Schroter RC (1969) Arterial wall shear and distribution of early atheroma in man. Nature 223:1159–1160

Caro CG, Fitzgerald JM, Schroter RC (1971) Atheroma and arterial wall shear stress. Observation, correlation, and proposal of a shear dependent masstransfer mechanism for atherogenesis. Proc Roy Soc B 177:109–159

Caro CG, Doorly DJ, Tarnawski M, Scott KT, Long Q, Dumoulin CL (1996) Non-planar curvature and branching of arteries and non-planar-type flow. Proc R Soc Lond A 452:185–197

Caro CG, Watkins NW, Sherwin SJ, Pitt R, Giordana S, Franke PT, Peiro J, Doorly DJ, Papaharilaou Y, Chesire N, Jackson M, Bicknall C (2002) Swirling circulatory and respiratory flow: biological/pathological implications. IFMBE Proc, EMBEC 2002, I8–I16

Caro CG (2009) Discovery of the role of wall shear in Atherosclerosis. Arterioscler Thromb Vasc Biol 29:158–161

Chen ZS, Fan YB, Deng XY, Xu Z (2009) Swirling flow can suppress flow disturbances in endovascular stents: a numerical study. Am Soc Artif Int Organ J 55(6):543–549

Chien S (2007) Mechanotransduction and endothelial cell homeostasis: the wisdom of the cell. Am J Physiol Heart Circ Physiol 292:H1209–H1224

Chiu JJ, Chien S (2011) Effects of disturbed flow on vascular endothelium: pathophysiological basis and clinical perspectives. Physiol Rev 91:327–387

De Bakey ME, Lawrie GM, Glaeser DH (1985) Patterns of Atherosclerosis and their Surgical Significance. Ann Surg 201:115–131

De Paola N, Gimbrone MA Jr, Davies PF, Dewey CF Jr (1992) Vascular endothelium responds to fluid shear stress gradients. Arterioscler Thromb 12(11):1254–1257

Ditlevsen PD, Giuliani P (2000) Anomalous scaling in a shell model of helical turbulence. Phys A 280:69–74

Ehrlich LW, Friedman MH (1977) Particle paths and stasis in unsteady flow through a bifurcation. J Biomech 10:561–568

Euler L (1775) Principia pro motusanguinis per arterias determinando. Opera posthumamathematica et physica anno 1844 detecta. Ediderunt P.H. Fuss et N. Fuss Petropoli; Apund Eggers et Socios

Fan Y, Xu Z, Jiang W, Deng X, Wang K, Sun A (2008) An S-type bypass can improve the hemodynamics in the bypassed arteries and suppress intimal hyperplasia along the host artery floor. J Biomech 41:2498–2505

Fatemi RS, Rittgers SE (1994) Derivation of shear rates from near-wall LDA measurements under steady and pulsatile flow conditions. J Biomech Eng 116(3):361–368

Frazin LJ, Lanza G, Vonesh M, Khasho F, Spitzzeri C, McGee S, Mehlman D, Chandran KB, Talano J, McPherson D (1990) Functional chiral asymmetry in descending thoracic aorta. Circulation 82(6):1985–1994

Frazin LJ, Vonesh MJ, Chandran KB, Shipkowitz T, Yaacoub AS, McPherson DD (1996) Confirmation and initial documentation of thoracic and abdominal aortic helical flow, An ultrasound study. Am Soc Artif Int Organ J 42(6):951–956

Friedman MH, Hutchins GM, Bargeron CB, Deters OJ, Mark FF (1981) Correlation between intimal thickness and fluid shear in human arteries. Atheroscler 39:425–436

Friedman MH, Bargeron CB, Deters OJ, Hutchins GM, Mark FF (1987) Correlation between wall shear and intimal thickness at a coronary artery branch. Atheroscler 68:27–33

Frydrychowicz A, Franc-ois CJ, Turski PA (2011) Four-dimensional phase contrast magnetic resonance angiography: potential clinical applications. Eur J Radiol 80:24–35

Galbraith CG, Skalak R, Chein S (1998) Shear stress induces spatial reorganization of the endothelial cell cytoskeleton. Cell Motil Cytoskelet 40:317–330

Gallo D, Steinman DA, Bijari PB, Morbiducci U (2012a) Helical flow in carotid bifurcation as surrogate marker of exposure to disturbed shear. J Biomech 45(14):2398–2404

Gallo D, De Santis G, Negri F, Tresoldi D, Ponzini R, Massai D, Deriu MA, Segers P, Verhegghe B, Rizzo G, Morbiducci U (2012b) On the use of in vivo measured flow rates as boundary conditions for image-based hemodynamic models of the human aorta. Implications for indicators of abnormal flow. Ann Biomed Eng 40(3):729–741

Gelfand BD, Epstein FH, Blackman BR (2006) Spatial and spectral eterogeneity of time-varying shear stress profiles in the carotid bifurcation by PC-MRI. J Magn Reson Imaging 24(6):1386–1392

Giddens DP, Zarins CK, Glagov S (1993) The role of fluid mechanics in the localization and detection of atherosclerosis. J Biomech Eng 115(4B):588–595

Glagov S, Zarins C, Giddens DP, Ku DN (1988) Hemodynamics and atherosclerosis, insights and perspective gained from studies of human arteries. Arch Pathol Lab Med 112:1018–1029

Goubergrits L, Affeld K, Fernandez-Britto J, Falcon L (2002) Atherosclerosis and flow in carotid arteries with authentic geometries. Biorheol 39(3–4):519–524

Grigioni M, Daniele C, Morbiducci U, Del Gaudio C, D'Avenio G, Balducci A, Barbaro V (2005) A mathematical description of blood spiral flow in vessels: application to a numerical study of flow in arterial bending. J Biomech 38:1375–1386

Haller G (2001) Distinguished material surfaces and coherent structures in three-dimensional fluid flows. Phys D 149:248–277

Harloff A, Albrecht F, Spreer J, Stalder AF, Bock J, Frydrychowicz A, Schollorn J, Hetzel A, Schumacher M, Hennig J, Markl M (2009) 3D blood flow characteristics in the carotid artery bifurcation assessed by flow-sensitive 4D MRI at 3T. Magn Reson Med 61:65–74

He X, Ku DN (1996) Pulsatile flow in the human left coronary artery bifurcation: average conditions. ASME J Biomech Eng 118(1):74–82

Himburg HA, Grzybowski DM, Hazel A, LaMack JA, Li XM, Friedman MH (2004) Spatial comparison between wall shear stress measures and porcine arterial endothelial permeability. Am J Physiol Heart Circ Physiol 286(5):H1916–H1922

Himburg HA, Friedman MH (2006) Correspondence of low mean shear and high harmonic content in the porcine iliac arteries. J Biomech Eng 128(6):852–856

Houston JG, Gandy SJ, Sheppard DG, Dick JBC, Belch JJF, Stonebridge PA (2003) Two-dimensional flow quantitative MRI of aortic arch blood flow patterns: effect of age, gender and presence of carotid atheromatous disease on the prevalence of spiral blood flow. J Magn Reson Imaging 18(2):169–174

Houston JG, Gandy SJ, Milne W, Dick JB, Belch JJ, Stonebridge PA (2004) Spiral laminar flow in the abdominal aorta: a predictor of renal impairment deterioration in patients with renal artery stenosis? Nephrol Dial Transplant 19(7):1786–1791

Hsiai TK, Cho SK, Wong PK, Ing M, Salazar A, Sevanian A, Navab M, Demer LL, Ho CM (2003) Monocyte recruitment to endothelial cells in response to oscillatory shear stress. Faseb J 17(12):1648–1657

Hyun S, Kleinstreuer C, Archie JP (2000) Computer simulation and geometric design of endarterectomized carotid artery bifurcations. Crit Rev Biomed Eng 28:53–59

Hyun S, Kleinstreuer C, Archie JP (2001) Computational particle-hemodynamics analysis and geometric reconstruction after carotid endarterectomy. Comp Biol Med 31:365–384

Hyun S, Kleinstreuer C, Longest PW, Chen C (2004) Particle-hemodynamics simulations and design options for surgical reconstruction of diseased carotid artery bifurcations. J Biomech Eng 126(4):118–195

Karino T, Goldsmith HL (1985) Particle flow behavior in models of branching vessels. II. Effects of branching angle and diameter ratio on flow patterns. Biorheol 22:87–104

Kessler M (2002) Biocompat. Nephrol Dial Transplant 17(7):32–44

Keynton RS, Evancho MM, Sims RL, Rodway NV, Gobin A, Rittgers SE (2001) Intimal hyperplasia and wall shear in arterial bypass graft distal anastomoses: an in vivo model study. J Biomech Eng 123(5):464–473

Kilner PJ, Yang GZ, Mohiaddin RH, Firmin DN, Longmore DB (1993) Helical and retrograde secondary flow patterns in the aortic arch studied by three-directional magnetic resonance velocity mapping. Circ 88:2235–2247

Kleinstreuer C, Hyun S, Buchanan JR, Longest PW, Archie JP, Truskey GA (2001) Hemodynamic parameters and early intimal thickening in branching blood vessels. Crit Rev Biomed Eng 29:1–64

Kroll MH, Hellums JD, McIntire LV, Schafer AL, Moake JL (1996) Platelets and shear stress. Blood 88(5):1525–1541

Ku DN, Giddens DP (1983) Pulsatile flow in a model carotid bifurcation. Arterioscler 3:31–39

Ku DN, Zarins CK, Giddens DP, Glagov S (1985) Hemodynamics of the normal human carotid bifurcation: in vitro and in vivo studies. Ultrasound Med Biol 11:13–26

Lee SW, Antiga L, Steinman DA (2009) Correlations among indicators of disturbed flow at the normal carotid bifurcation. J Biomech Eng 131(6):061013-1-7

Liu X, Pu F, Fan Y, Deng X, Li D, Li S (2009) A numerical study on the flow of blood and the transport of LDL in the human aorta: the physiological significance of the helical flow in the aortic arch. Am J Physiol Heart Circ Physiol 297:H163–H170

Liu X, Fan Y, Deng X (2010) Effect of spiral flow on the transport of oxygen in the aorta: a numerical study. Ann Biomed Eng 38:917–926

Liu X, Fan Y, Deng X, Zhan F (2011) Effect of non-Newtonian and pulsatile blood flow on mass transport in the human aorta. J Biomech 44(6):1123–1131

Long DS, Smith ML, Pries RA, Ley K, Damiano ER (2004) Microviscometry reveals reduced blood viscosityand altered shear rate and shear stress profiles in microvessels after hemodilution. Proc Natl Acad Sci USA 101(27):10060–10065

Longest PW, Kleinstreuer C (2000) Computational haemodynamics analysis and comparison study of arterio-venous grafts. J Med Eng Technol 24(3):102–110

Lorenz R, Benk C, Stalder AF, Korvink JG, Hennig J, Matkl M (2012) Closed circuit MR compatible pulsatile pump system using a ventricular assist device and pressure control unit. Magn Reson Med 67:258–268

Ma P, Li X, Ku DN (1997) Convective mass transfer at the carotid bifurcation. J Biomech 30:565–571

Malek AM, Alper SL, Izumo S (1999) Hemodynamic shear stress and its role in atherosclerosis. J Am Med Ass 282:2035–2042

Markl M, Wegent F, Zech T, Bauer S, Strecker C, Schumacher M, Weiller C, Hennig J, Harloff A (2010) In vivo wall shear stress distribution in the carotid artery: effect of bifurcation geometry, internal carotid artery stenosis, and recanalization therapy. Circ Cardiov Imaging 3:647–655

Marsden AL, Feinstein JA, Taylor CA (2008) A computational framework for derivative-free optimization of cardiovascular geometries. Comp Methods Appl Mech Eng 197(21–24):1890–1905

Massai D, Soloperto G, Gallo D, Xu XY, Morbiducci U (2012) Shear-induced platelet activation and its relationship with blood flow topology in a numerical model of stenosed carotid bifurcation. Eur J Mech-B/Fluids 35:92–101

Moffatt HK (1969) The degree of knottedness of tangled vortex lines. J Fluid Mech 35(1):17–29

Moffatt HK, Tsinober A (1992) Helicity in laminar and turbulent flow. Annu Rev Fluid Mech 24:281–312

Moore JE Jr, Xu C, Glagov s, Zarins CK, Ku DN (1994) Fluid wall shear stress measurements in a model of the human abdominal aorta: oscillatory behavior and relationship to atherosclerosis. Atheroscler 110(2):225–240

Morbiducci U, Lemma M, Ponzini R, Boi A, Bondavalli L, Antona C, Montevecchi FM, Redaelli A (2007a) Does flow dynamics of the magnetic vascular coupling for distal anastomosis in coronary artery bypass grafting contribute to the risk of graft failure? Int J Artif Organs 30:628–639

Morbiducci U, Ponzini R, Grigioni M, Redaelli A (2007b) Helical flow as fluid dynamic signature for atherogenesis in aortocoronary bypass, a numeric study. J Biomech 40:519–534

Morbiducci U, Ponzini R, Rizzo G, Cadioli M, Esposito A, De Cobelli F, Del Maschio A, Montevecchi FM, Redaelli A (2009a) In vivo quantification of helical blood flow in human aorta by time-resolved three-dimensional cine phase contrast MRI. Ann Biomed Eng 37:516–531

Morbiducci U, Ponzini R, Nobili M, Massai D, Montevecchi FM, Bluestein D, Redaelli A (2009b) Blood damage safety of prosthetic heart valves. Shear-induced platelet activation and local flow dynamics: a fluid-structure interaction approach. J Biomech 42(12):1952–1960

Morbiducci U, Gallo D, Ponzini R, Massai D, Antiga L, Redaelli A, Montevecchi FM (2010) Quantitative analysis of bulk flow in image-based haemodynamic models of the carotid bifurcation: the influence of outflow conditions as test case. Ann Biomed Eng 38(12):3688–3705

Morbiducci U, Ponzini R, Rizzo G, Cadioli M, Esposito A, Montevecchi FM, Redaelli A (2011) Mechanistic insight into the physiological relevance of helical blood flow in the human aorta: an in vivo study. Biomech Model Mechano biol 10:339–355

Morbiducci U, Ponzini R, Rizzo G, Biancolini ME, Iannaccone F, Gallo D, Redaelli A (2012) Synthetic dataset generation for the analysis and the evaluation of image-based hemodynamics of the human aorta. Med Biol Eng Comput 50(2):145–154

Morbiducci U, PonziniR, Gallo D, Bignardi C, Rizzo G (2013) Inflow boundary conditions for image-based computational hemodynamics: impact of idealized versus measured velocity profiles in the human aorta. J Biomech 46(1):102–109

Papathanasopoulou P, Zhao S, Köhler U, Robertson MB, Long Q, Hoskins P, Yun XuX, Marshall I (2003) MRI measurement of time-resolved wall shear stress vectors in a carotid bifurcation model, and comparison with CFD predictions. J Magn Reson Imaging 17:153–162

Pedersen EM, Agerbaek M, Kristensen IB, Yoganathan AP (1997) Wall shear stress and early atherosclerotic lesions in the abdominal aorta in young adults. Eur J Vasc Endovasc Surg 13:443–451

Perktold K, Resch M (1990) Numerical flow studies in human carotid artery bifurcations: basic discussion of the geometric factor in atherogenesis. J Biomed Eng 12(2):111–123

Pritchard WF, Davies PF, Derafshi Z, Polacek DC, Tsao R, Dull RO, Jones SA, Giddens DP (1995) Effects of wall shear stress and fluid recirculation on the localization of circulating monocytes in a three-dimensional flow model. J Biomech 28(12):1459–1469

Santilli SM, Stevens RB, Anderson JG, Payne WD, Caldwell MD (1995) Transarterial wall oxygen gradients at the dog carotid bifurcation. Am J Physiol Heart Circ Physiol 268:H155–H161

Shaaban AM, Duerinckx AJ (2000) Wall shear stress and early atherosclerosis: a review. Am J Roentgenol 174:1657–1665

Shadden SC, Lekien F, Marsden JE (2005) Definition and properties of Lagrangian coherent structures from finite-time Lyapunov exponents in two-dimensional aperiodic flows. Phys D 212(3–4):271–304

Shadden SC, Taylor CA (2008) Characterization of coherent structures in the cardiovascular system. Ann Biomed Eng 36(7):1152–1162

Shtilman L, Levich E, Orszag SA, Pelz RB, Tsinober A (1985) On the role of helicity in complex fluid flows. Phys Lett 113A:32–37

Sluimer JC, Gasc JM, van Wanroij JL, Kisters N, Groeneweg M, SollewijnGelpke MD, Cleutjens JP, van den Akker LH, Corvol P, Wouters BG, Daemen MJ, Bijnens AP (2008) Hypoxia, hypoxia-inducible transcription factor, and macrophages in human atherosclerotic plaques are correlated with intraplaque angiogenesis. J Am Coll Cardiol 51:1258–1265

Steinman DA (2000) Simulated pathline visualization of computed periodic blood flow patterns. J Biomech 33(5):623–628

Stonebridge PA, Hoskins PR, Allan PL, Belch JF (1996) Spiral laminar flow in vivo. Clin Sci 91:17–21

Sun N, Wood NB, Hughes AD, Thom SAM, Xu XY (2007) Effects of transmural pressure and wall shear stress on LDL accumulation in the arterial wall: a numerical study using a multilayered model. Am J Physiol Heart Circ Physiol 292:H3148–H3157

Tambasco M, Steinman DA (2001) Calculating particle-to-wall distances in unstructured computational fluid dynamic models. Appl Math Model 25:803–814

Tambasco M, Steinman DA (2002) On assessing the quality of particle tracking through computational fluid dynamic models. J Biomech Eng 124:166–175

Taylor CA, Steinman DA (2010) Image-based modeling of blood flow and vessel wall dynamics: applications, methods and future directions. Ann Biomed Eng 38(3):1188–1203

Vetel J, Garon A, Pelletier D (2009) Lagrangian coherent structures in the human carotid artery bifurcation. Exp Fluid 46(6):1067–1079

Womersley JR (1955) Method for the calculation of velocity, rate of flow and viscous drag in arteries when the pressure gradient is known. J Physiol 127:553–563

Yoshizumi M, Abe J, Tsuchiya K, Berk BC, Tamaki T (2003) Stress and vascular responses: atheroprotective effect of laminar fluid shear stress in endothelial cells: possible role of mitogen-activated protein kinases. J Pharmacol Sci 91:172–176

Zhan F, Fan Y, Deng X (2010) Swirling flow created in a glass tube suppressed platelet adhesion to the surface of the tube: Its implication in the design of small-caliber arterial grafts. Thromb Res 125(5):413–418

Zhao SZ, Ariff B, Long Q, Hughes AD, Thom SA, Stanton AV, Xu XY (2002) Inter-individual variations in wall shear stress and mechanical stress distributions at the carotid artery bifurcation of healthy humans. J Biomech 35(10):1367–1377

Zheng T, Fan Y, Xiong Y, Jiang W, Deng X (2009) Hemodynamic performance study on small diameter helical grafts. Am Soc Artif Int Organ J 55:192–199